Tension of freely suspended fluid filaments

M. Morys, T. Trittel, A. Eremin, P. Murphy, and R. Stannarius

Tension of freely suspended fluid filaments

M. Morys[1], T. Trittel[1], A. Eremin[1], P. Murphy[2], and R. Stannarius[1]

[1]*Otto von Guericke University Magdeburg, Institute of Experimental Physics,*
Universitätsplatz 2, D-39106 Magdeburg, Germany,
[2]*Liquid Crystal Institute, Kent State University P.O. Box 5190, Kent, OH 44242-0001, USA.*

Stable fluid filaments with diameters of several micrometers and slenderness ratios well above 1000 are unique objects formed by some liquid crystalline phases of bent-core mesogens. We present a technique to determine filament tensions from their deflection under defined loads. A strong temperature dependence is observed, with a minimum near the clearing temperature. Both the non-linear relation between filament tension and diameter and the substantial increase of the tension with lower temperatures indicate contributions of volume terms, in addition to surface capillary forces. We discuss a model that relates these bulk terms to elastic forces, originating from the undulated smectic layer structure. This model can explain the origin of the filament stability.

PACS numbers: 62.10.+s, 61.30.-v,

I. INTRODUCTION

Freely suspended fluid filaments are among the most exotic structures formed by liquid crystalline materials [1–18]. Most of these unique structures are found in some mesophases of bent-core smectogens. Bent-core materials are particularly interesting because they can form chiral phases of achiral molecules, which may be ferroelectric or antiferroelectric [19]. A promising application of liquid crystal filaments e.g. as optical wave guides has been proposed recently [16]. The reason for their stability is not fully understood (a molecular layer structure appears to be insufficient for a stabilization) and little is known about their fundamental mechanical properties. Such filaments represent either single cylindrical fibers or bundles of fibrils of about 2 μm diameter. The smectic layers are wrapped around the fibril axes [6, 8]. The material can flow freely along the axis. When the filament length is varied, its cross section remains unchanged, and material is exchanged with the bulk reservoir. The bundle thickness can range from a few micrometers to 100 μm and more, slenderness ratios (length to diameter) of 1000 and more can be achieved. Filaments in equilibrium are straightened by their tension.

Fluid filaments are unique in two aspects: first, they are not subject to the Rayleigh-Plateau instability which causes cylinders of ordinary liquids to decompose into droplets when their aspect ratio exceeds π. Second, as we will show in this study, the filament tension is not caused by capillary forces alone. In addition to the surface tension, bulk forces related to the complex smectic molecular arrangement contribute to the macroscopic filament tension.

Earlier mechanical and electrical studies explored the dynamical properties of such filaments [6, 7, 12]. However, still very little is known about their mechanical characteristics. In plucking experiments [7], filaments of a few millimeters length were deflected by an electric field. After the field was switched off, they performed damped oscillations, which provided information on mechanical parameters, e.g. the filament tension Σ.

Later, mechanical resonances were studied under continuous excitation with sound waves [12]. If one neglects contributions of the internal filament structure, a plausible assumption is to set Σ equal to the specific surface energy per filament length [3, 4], $2\pi r\sigma$ (radius r, surface tension σ). Our experimental data contradict this simple model and indicate the existence of additional forces. Bailey et al. [15] proposed a model that includes bulk elastic terms. An alternative model, that also considers bulk energy contributions, but of different nature, was put forward recently by Eremin et al. [18].

Still, there remains the non-satisfactory situation that filament tensions have not been measured directly. Cantilever methods [8, 17] are apparently too inaccurate. In this study, we describe a direct measurement technique, we determine the temperature dependence of $\Sigma(T)$. The method avoids the problems of previous studies.

Filaments are suspended horizontally to measure their deflection by gravity. Under their own weight, filaments deflect by few micrometers only [20], this deformation can be ignored here. We attach loads (glass or metal microbeads) of known weights, that stick to the filaments by capillary forces. Filaments are drawn in a $6\times6\times6$ cm^3 thermobox (temperature range up to 200°C) and observed through quartz windows with a long range microscope (Questar QM 100) [9].

The chemical composition of the investigated material is shown in Fig. 1. The substance has a phase sequence isotropic 160°C PM-SmCP 143°C SmCP 90°C cryst. where SmCP is a simple polar tilted smectic phase and PM-SmCP is a polar tilted smectic phase with undulated layer structure [21]. Stable filaments can be prepared only in the high temperature PM-SmCP phase.
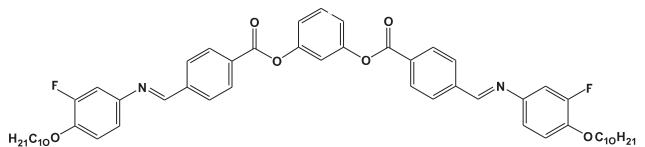

FIG. 1: Chemical structure of the investigated material
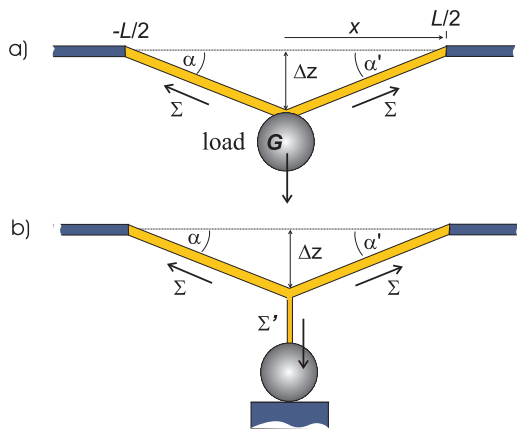
FIG. 2: Geometries for the measurement of filament tensions: a) deflection under the weight of a glass sphere, b) force balance of three filaments

The filaments are prepared near the clearing point, and drawn to lengths ℓ of a few millimeters. Filament cross sections are not always circular, we make an elliptical approximation, the half axes a, b are determined by rotating the filament about its long axis before the load is attached [20]. Then a support plate carrying a glass or steel bead is approached from below until the bead touches the filament. When the dish is lowered again, the bead detaches from the support dish and sticks to the filament. The geometry is sketched in Fig. 2a, and the experimental realization is shown in Fig. 3a. Glass microbeads with submillimeter size and weights of the order of a few μN (e.g. about 3 μN for 0.6 mm diameter) are sufficient to distort filaments with diameters the order of ≈ 100 μm. The weight G is obtained from the bead diameter and the known density of the glass. At thick filaments, we attach more than one bead to obtain larger deflections.

The equilibrium inclination angles $\alpha \approx \alpha'$ of the filament segments are measured and the filament tension Σ is found from the force balance

$$G = (\sin\alpha + \sin\alpha')\Sigma. \tag{1}$$

A difference to similar measurements of elastomer fibers [22] is that the angles α, α' do not change when the distance between the lateral holders is varied. The fluid filament elongates or shortens correspondingly, it adjusts its length by material flow out of or into the meniscus.

The only assumption in this model is that the forces are in equilibrium. The sharp bend of the filament at the position of the bead does not contribute to the force balance, all relevant forces in the filaments act in axial directions. A magnified view of the contact between the filament and the bead is seen in Fig. 4a. The local structure of the filament is almost uninfluenced by the load, only a small meniscus connects filament and load. Except for the bend at this connection, the filaments are perfectly straight.

This technique can be varied slightly for the assessment of the radius dependence, by evaluating forces be-
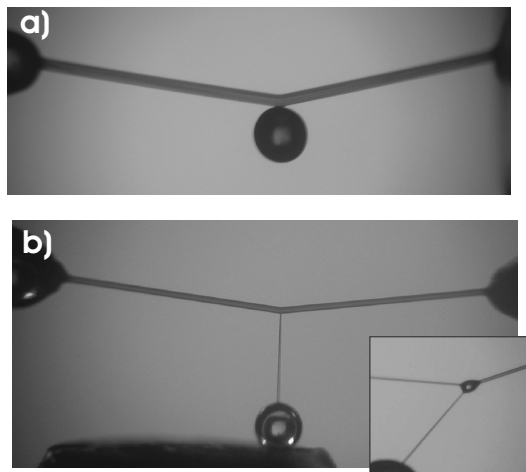

FIG. 3: a) Image of a filament of 152 μm diameter with an attached glass bead. The distance between the two supports is 6 mm, the temperature is 2.2 K below the melting point. b) Bent filament of 80 μm diameter with a branch to a thin, nearly vertical filament (20 μm diameter). The inset shows three connected filaments with different diameters (8 μm (top left), 15 μm (right) and 7 μm (bottom left). The tensions determined from the angles relate as 0.63 : 1.0 : 0.49, resp.

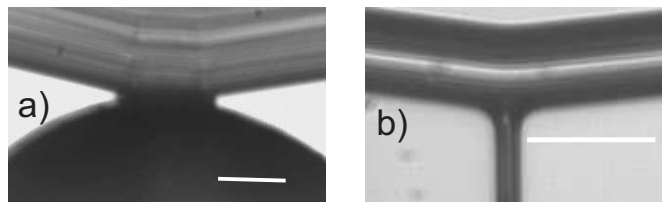

FIG. 4: a) Contact zone of a glass sphere (diameter 788 μm) with the vertical filament, the temperature is 2.2 K below the melting point. b) Three filament branches in contact. The diameter of the thin vertical branch is 22 μm. White bars mark 100 μm length.

tween tree connected filaments: If a bead is too heavy, it detaches from the filament and creates a thinner filament branch of radius r_2. A triangular connection forms, as seen in Figs. 3b and 4b and in the sketch in Figure 2b. Three tensions establish a force equilibrium. Except for a small meniscus at the connection, there are no distortions of the filament structures. In the simplest case, where both upper branches are of equal radius r_1 and the third filament has a radius r_2 (Fig. 3b), α equals α' and $\Sigma(r_2) = 2\Sigma(r_1)\sin\alpha$ The radii and the angles between the three filaments provide a direct test of the capillary force hypothesis. If $\Sigma(r_2)/\Sigma(r_1) = r_2/r_1$ for all r_1, r_2, then the tension is proportional to the filament perimeter, i.e. it is likely to reflect a pure surface property. A nonlinear dependence indicates that the tension contains terms related to the bulk. In a cylindrical filament such bulk terms would give $\Sigma(r) \propto r^2$. Combinations of linear and quadratic terms indicate a superposition of volume and surface contributions. If the filament cross sections

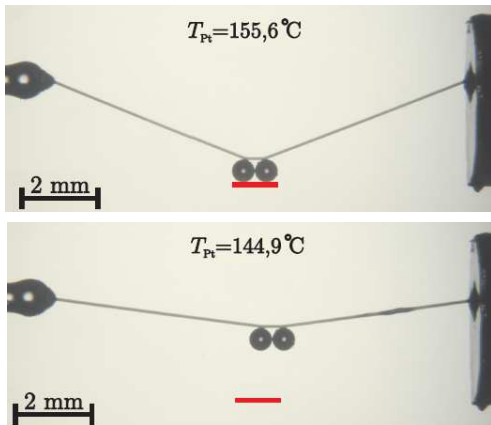are elliptical, one has to replace $2\pi r$ by the true perimeter P.

FIG. 5: Filament deflection under load. The horizontal bar marks the initial position at 155.6°C. All changes are fully reversible. After temperature changes the force equilibrium is established within less than one minute.

The strong temperature characteristics of the tension Σ produces a reversible geometrical change of the fluid filament during heating/cooling (Fig. 5). Qualitative results are shown in Fig. 6 for two typical filaments. Experimental uncertainty is somewhat larger at low temperatures where the deflection angles are smaller at given weights. In both filaments, the forces strongly increase with decreasing temperature. In some filaments (cf. 6b), we observe a slight increase of Σ also towards the clearing point. This reversed slope in the vicinity of the clearing temperature is not found in all filaments, often filaments break on approaching the phase transition. Both filaments in Fig. 6 are slightly elliptical in the cross section. We take the perimeter of an ellipse and make a correction that takes the corrugations of the filament surface [12] into account. When the bundle consists of much smaller, cylindrical fibrils, then its surface can be considered as an array of parallel cylinders. Thus we replace each cylinder diameter by half the circumference of a cylinder to approximate the real bundle perimeter. This yields a correction factor of $\pi/2$ as a rough estimate. Further we assume a surface tension of 0.02 N/m (σ of similar materials are found in Refs. [23, 24]), and arrive at capillary forces of 6.1 μN (a) and 9.7 μN (b), resp. (dashed lines). The excess forces, in particular the increase by a factor of about three at low temperatures, cannot be explained by capillarity.

In Fig. 7, we compare the tensions of filaments of different thicknesses at two fixed temperatures. The expected contribution of the surface tension is indicated by a straight line. Only for very thin filaments, it represent a satisfactory approximation. For thick filaments, a quadratic contribution to $\Sigma(r)$ dominates. The data scatter too much to allow a combined fit of both the linear and quadratic terms of these curves. Instead, we
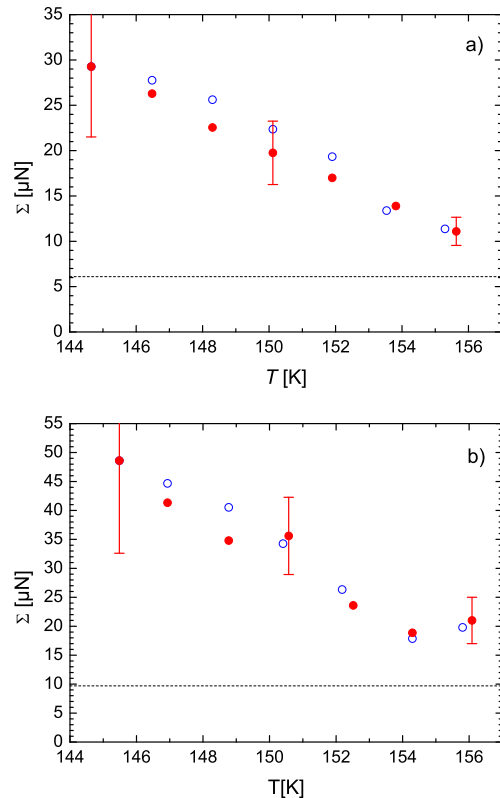

FIG. 6: Temperature dependent tensions $\Sigma(T)$ of two representative thick filaments during cooling (solid, red) and heating (open, blue), (a) $\ell = 10.09$ mm, $a = 69$ μm, $b = 54$ μm, two steel beads of 0.4 mm diameter attached, (b) $\ell = 8.5$ mm, $a = 114$ μm, $b = 82.5$ μm, one 0.8 mm glass bead attached. The dashed lines indicate the contributions related to capillary forces with an assumed $\sigma = 0.02$ N/m.
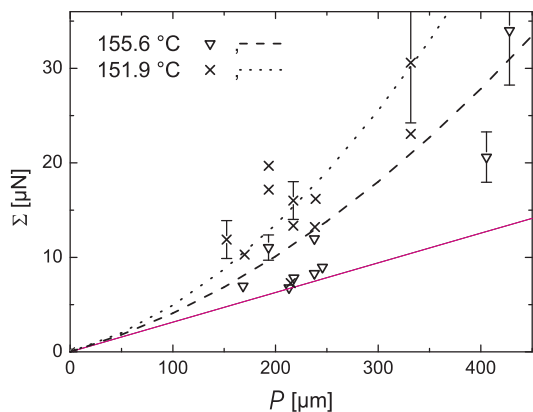

FIG. 7: Dependence of the filament tension upon the perimeter, calculated from the two half axes a,b with a corrugation correction factor of $\pi/2$ (see text) for all filaments. The solid line indicates the capillary force calculated with $\sigma = 0.02$ N/m, dots/dashes are fits to Eq. (2).

fitted the filament tensions to an equation

$$\Sigma = \sigma P(a,b) + \eta \pi a b, \qquad (2)$$

with a temperature independent $\sigma = 0.02$ N/m. The coefficient η of the volume contribution to Σ represents an energy density. This bulk term dominates in thick filaments (in cylindrical filaments when $r > 2\sigma/\eta$). The resulting $\eta(T)$ curve is given in Fig. 8. The scattering of the data is mainly due to varying surface corrugations. Fig. 8 shows that the bulk parameter η strongly increases with decreasing temperature.
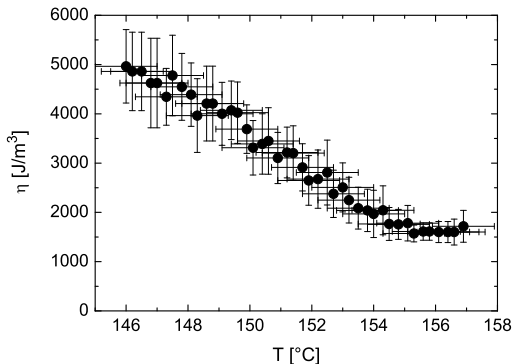

FIG. 8: Temperature dependence of the coefficient η [Eq. 2] of the volume contribution to the filament tension.

This trend of a stronger than linearly increasing ratio of tensions with increasing filament thickness (Fig. 7) is confirmed qualitatively and quantitatively with interconnected filaments of different radii (Figs. 2b,3b). All experimental data support the interpretation that the bulk term increases with decreasing temperature, whereas the surface tension contributions are rather constant.
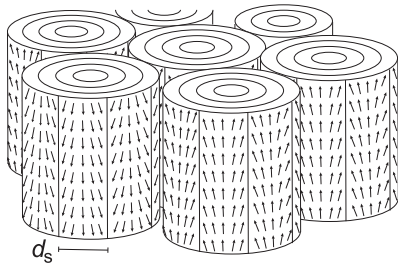

FIG. 9: Model of the polarization splay stripes in the fibers. Arrows symbolize the spontaneous polarization $\vec{p}$. The c-director is perpendicular to $\vec{p}$ in the layer plane. The sketched configuration complies with the observation that the filaments generate an axially polarized optical second harmonic [18, 25].

The bulk term has to be interpreted as an energy nec-essary to create filament volume from bulk material. We propose that it is related to the two-dimensional structure of striped domains in the polarization-modulated undulated layer phase [26]. The equilibrium stripe width d_0 varies from less than 100 nm near the clearing point to about micrometer size near the low temperature SmCP phase. In the fibers, the stripes are in axial direction as sketched in Fig. 9 [25]. Because of the spontaneous polarization splay, a term of the form $K\left\{1/d_s - 1/d_0(T)\right\}^2$ approximates a bend elastic contribution to the free energy density, where $d_0(T)$ defines the equilibrium bulk value, $K \approx 10$ pN is a corresponding elastic constant, d_s is the actual stripe width. We assume that the stripe width d_s in the fibers is fixed, imposed either by the boundary conditions or by the curved layer arrangement, or imprinted during preparation. Then, cooling of the filaments leads to a mismatch of $d_0(T)$ and d_s. With $d_0 \approx 1$ μm at low temperatures and $d_s \approx 50$ nm, the excess free energy per volume becomes ≈ 4 kJ/m^3. This agrees with the order of magnitude of the measured $\eta(T)$ in the filament tension (Fig. 8). Of course, for an exact quantitative description this model needs refinement, electric self-energies [14, 15] and energies related to the defect lines at the stripe boundaries should be considered as well. Measurements of the polar order of the filaments by optical Second Harmonics interferometry [18] strongly support the model described here. Freeze-fracture and electron microscopy might be useful for a direct observation of the stripes in fiber geometry. Further evidence that the bulk term originates from the particular smectic structure comes from a comparison with filaments of columnar liquid crystal phases. In a vibration analysis, it was established that the filament tension of the latter originates from surface contributions alone [3, 4].

Summarizing, the tension of liquid crystal filaments of the investigated bent-core mesogens is composed of two contributions: capillary forces as in ordinary liquids and an additional term that may originate from the 2D molecular arrangement in the fibrils. The assumption of a fixed number of splay stripes in the individual fibers provides a reasonable explanation why the filaments in PM-SmCP are not subject to the Rayleigh-Plateau instability, unlike most other smectic phases. The striped structure lets the molecular arrangement in the filaments appear more similar to 1D columns, rather than 2D extended layers of typical smectic phases.

[1] D. V. Winkle and N. Clark, *Phys. Rev. Lett.* **48** 1407 (1982).

[2] C. Safinya, K. Liang, W. Varady, N. Clark, and G. An-

dersson, *Phys. Rev. Lett.* **53** 1172 (1984).

[3] M. Gharbia, A. Gharbi, M. Cagnon, and G. Durand, *J. Phys. (France)* **51** 1355 (1990).

[4] M. Gharbia and A. Gharbi, *Surf. Sci.* **317** L1136 (1994).

[5] G. Pelzl et al., *Liq. Cryst.* **26**, 135 (1999)

[6] A. Jákli, D. Krüerke, G.G. Nair, *Phys. Rev. E* **67**, 051702 (2003)

[7] R. Stannarius, A. Nemeş, and A. Eremin. *Phys. Rev. E* **72**, 020702(R) (2005).

[8] A. Eremin, A. Nemeş, R. Stannarius, M. Schulz, H. Nádasi, W. Weissflog, *Phys. Rev. E* **71**, 031705 (2005)

[9] A. Nemeş, A. Eremin, R. Stannarius, M. Schulz, and W. Weissflog. *Phys. Chem. Chem. Phys.* **8**, 469 (2006).

[10] A. Nemeş, A. Eremin, and R. Stannarius. *Mol. Cryst. Liq. Cryst.* **449**, 179 (2006).

[11] A. Eremin et al., *Liq. Cryst.* **33**, 789 (2006).

[12] J. Petzold et al., *Soft Matter* **5**, 3120 (2009).

[13] A. Nemeş, PhD thesis, Magdeburg (2008).

[14] C. Bailey, PhD thesis, Kent, OH (2008).

[15] C. Bailey, E.C. Gartland and A. Jákli, *Phys. Rev. E* **75**, 031701 (2007)

[16] J. Fontana, C. Bailey, W. Weissflog, I. Jánossy, and A. Jákli, *Phys. Rev. E* **80**, 032701 (2009)

[17] C. Bailey, M. Murphy, A. Eremin, W. Weissflog, and A. Jákli, *Phys. Rev. E*, **81** 031708 (2010)

[18] A. Eremin et al., *Phys. Rev. Lett.*, **109**, 017801 (2012).

[19] T. Niori, T. Sekine, J. Watanabe, T. Furukawa, and H. Takezoe, *J. Mater. Chem.* **6**, 1231 (1996); T. Sekine et al., *Jpn. J. Appl. Phys.* **36**, 6455 (1997).

[20] M. Morys, T. Trittel, and R. Stannarius, *Ferroelectrics* **431**, 129 (2012).

[21] M. Nakata et al., *Phys. Rev. E* **71**, 011705 (2005).

[22] R. Stannarius et al., *Soft Matter* **8** 1858, (2012).

[23] P. Mach et al., *Langmuir* **14**, 4330 (1998).

[24] H. Schüring, C. Thieme, and R. Stannarius. *Liq. Cryst.* **28**, 241 (2001).

[25] U. Kornek, Thesis, Magdeburg 2011.

[26] D. A. Coleman et al., *Science* **301**, 1204 (2003).